



Photochemical age of air pollutants, ozone, and secondary organic aerosol in transboundary air observed on Fukue Island, Nagasaki, Japan

Satoshi Irei^{1,a}, Akinori Takami¹, Yasuhiro Sadanaga², Susumu Nozoe^{1,b}, Seichiro Yonemura³, Hiroshi Bandow², and Yoko Yokouchi¹

¹National Institute for Environmental Studies, 16-2 Onogawa, Tsukuba, Ibaraki 305-8506, Japan

²Department of Applied Chemistry, Graduate School of Engineering, Osaka Prefecture University, 1-1 Gakuencho, Naka-ku, Sakai, Osaka 599-8531, Japan

³National Institute for Agro-Environmental Sciences, 3-1-3 Kannondai, Tsukuba, Ibaraki 305-8604, Japan

^apresent address: Department of Biology, Chemistry, and Marine Science, University of the Ryukyus, 1 Senbaru, Nishihara, Okinawa 903-0213, Japan

^bpresent address: National Museum of Emerging Science and Innovation, Aomi 2-3-6, Koto, Tokyo 135-0064, Japan

Correspondence to: Satoshi Irei (satoshi.irei@gmail.com)

Received: 16 October 2015 – Published in Atmos. Chem. Phys. Discuss.: 15 January 2016

Revised: 31 March 2016 – Accepted: 1 April 2016 – Published: 13 April 2016

Abstract. To better understand the secondary air pollution in transboundary air over westernmost Japan, ground-based field measurements of the chemical composition of fine particulate matter ($\leq 1\ \mu\text{m}$), mixing ratios of trace gas species (CO , O_3 , NO_x , NO_y , *i*-pentane, toluene, and ethyne), and meteorological elements were conducted with a suite of instrumentation. The CO mixing ratio dependence on wind direction showed that there was no significant influence from primary emission sources near the monitoring site, indicating long- and/or mid-range transport of the measured chemical species. Despite the considerably different atmospheric lifetimes of NO_y and CO , these mixing ratios were correlated ($r^2 = 0.67$). The photochemical age of the pollutants, $t[\text{OH}]$ (the reaction time \times the mean concentration of OH radical during the atmospheric transport), was calculated from both the NO_x/NO_y concentration ratio (NO_x/NO_y clock) and the toluene/ethyne concentration ratio (hydrocarbon clock). It was found that the toluene/ethyne concentration ratio was significantly influenced by dilution with background air containing 0.16 ppbv of ethyne, causing significant bias in the estimation of $t[\text{OH}]$. In contrast, the influence of the reaction of NO_x with O_3 , a potentially biasing reaction channel on $[\text{NO}_x]/[\text{NO}_y]$, was small. The $t[\text{OH}]$ values obtained with the NO_x/NO_y clock ranged

from 2.9×10^5 to $1.3 \times 10^8\ \text{h molecule cm}^{-3}$ and were compared with the fractional contribution of the $m/z\ 44$ signal to the total signal in the organic aerosol mass spectra (f_{44} , a quantitative oxidation indicator of carboxylic acids) and O_3 mixing ratio. The comparison of $t[\text{OH}]$ with f_{44} showed evidence for a systematic increase of f_{44} as $t[\text{OH}]$ increased, an indication of secondary organic aerosol (SOA) formation. To a first approximation, the f_{44} increase rate was $(1.05 \pm 0.03) \times 10^{-9} \times [\text{OH}]\ \text{h}^{-1}$, which is comparable to the background-corrected increase rate observed during the New England Air Quality Study in summer 2002. The similarity may imply the production of similar SOA component, possibly humic-like substances. Meanwhile, the comparison of $t[\text{OH}]$ with O_3 mixing ratio showed that there was a strong proportional relationship between O_3 mixing ratio and $t[\text{OH}]$. A first approximation gave the increasing rate and background mixing ratio of ozone as $(3.48 \pm 0.06) \times 10^{-7} \times [\text{OH}]\ \text{ppbv h}^{-1}$ and 30.7 ppbv, respectively. The information given here can be used for prediction of secondary pollution magnitude in the outflow from the Asian continent.

1 Introduction

During the last decade, the dramatic growth of the Chinese economy has increased emission of air pollutants such as volatile organic compounds, particulate matter (PM), and nitrogen oxides (NO_x), which is the sum of nitrogen monoxide (NO) and nitrogen dioxide (NO_2). In northeast Asia, air masses generally move from west to east, and therefore pollutants emitted on continental China are frequently carried to Japan. The influence of air pollution is becoming severe in rural areas of westernmost Japan, such as Fukue Island. Atmospheric oxidation of primary pollutants produces secondary pollutants, such as ozone (O_3) and secondary particulate organic matter (also known as secondary organic aerosol or SOA), which is formed by oxidation of volatile organic precursors. A better understanding of these secondary pollutants is important not only for purely scientific reasons but also because such pollutants are a matter of great public concern. SOA is one of the least understood subjects in atmospheric chemistry (Ebben et al., 2014), despite the fact that it has been studied extensively due to its potential adverse effects on human health and its role in cloud condensation. Although state-of-the-art techniques, such as aerosol mass spectrometry, have substantially improved our understanding of SOA (Zhang et al., 2005; Jimenez et al., 2009), many questions about SOA still remain, such as its constituents, production mechanisms, and fates.

To understand SOA, we must evaluate the progress of the chemical reactions of its constituents. The progress of photochemical reactions in the atmosphere has frequently been evaluated in terms of a “photochemical age”, designated $t[\text{OH}]$, which can be derived from non-methane hydrocarbon (NMHC) ratios (Roberts et al., 1984; Rudolph and Johnen, 1990) and from NO_x ratio to total odd nitrogen (NO_y) (Parrish et al., 1992). Recent field studies combining aerosol mass spectrometry measurements and determination of $t[\text{OH}]$ have provided new information about photochemically produced SOA (de Gouw et al., 2005; Takegawa et al., 2006; Kleinman et al., 2007; Liggio et al., 2010). Our previous field studies conducted on Fukue Island in Japan demonstrated a systematic trend for the fractions of carboxylate in the organic aerosol (f_{44}) with $t[\text{OH}]$, evidence of SOA production (Irei et al., 2014). However, the study period was short (only 10 days), and a longer observation period is necessary to obtain more-convincing evidence of SOA production. Furthermore, inconsistent results regarding the association between SOA production and $t[\text{OH}]$ were observed at the same location during a different time period (Irei et al., 2015). The study described in this paper is an extension of our previous studies, and the objective was to deepen our understanding of the association between oxidation products (SOA and O_3) and $t[\text{OH}]$ in transboundary air.

2 Experiment

Field measurements were conducted from December 2010 to May 2011 at the Fukue atmospheric monitoring station (32.8°N , 128.7°E), a rural site on the northwestern peninsula of Fukue Island, Nagasaki Prefecture, Japan (Fig. 1). As mentioned earlier, data collected during a 10-day observation period in December 2010 have already been reported, and the reported results are a part of data in this study. The monitoring station is $\sim 1 \text{ km}$ away from the residential area of the peninsula and is $\sim 60 \text{ m}$ higher in altitude. The site is located between small pastures. Possible sources of anthropogenic emissions of fine aerosol and trace gas species include agricultural waste burning, home incinerators, automobiles occasionally passing by the station, and tractors sometimes mowing the pastures. For all the measurements the ambient air was measured or sampled 1–3 m above the rooftop of the station (3–5 m height from the ground). An independent sampling line was assembled for each chemical species measurement. The ambient air was sampled at 1 L min^{-1} through $5 \text{ m} \times 0.25 \text{ in. o.d.}$ PTFE tubing for the CO and O_3 measurements and at 0.5 L min^{-1} through the same type of tubing for the NO_x and NO_y measurements, respectively. A molybdenum converter for the NO_y measurements was set at the inlet of sampling line. For the particle and NMHC measurements, the ambient air was suctioned at 3 and 5 L min^{-1} at the first stage through the sampling lines of $\sim 4 \text{ m} \times 0.5 \text{ in. o.d.}$ and $\sim 10 \text{ m} \times 0.625 \text{ in. o.d.}$ stainless steel tubing (GL Science, Japan), respectively. The measurements were then made by sampling a part of the flowing air. For the particle measurements only, a $\text{PM}_{2.5}$ cyclone separator (URG 2000-30ED, URG Corp. Chapel Hill, NC, USA) was attached to the inlet of the sampling line to cut off particles larger than $\text{PM}_{2.5}$.

The 10 min average chemical composition of fine aerosol ($\sim \text{PM}_{1.0}$) was measured with an Aerodyne quadrupole aerosol mass spectrometer (AMS; Aerodyne Research Inc., Billerica, MA, USA). Details of the instrumentation and the method for determination of chemical species concentrations are described elsewhere (Jayne et al., 2000; Allan et al., 2004). The AMS was calibrated approximately once a month with 350 nm dried ammonium nitrate particles for determination of ionization efficiencies. The temperature of the flash vaporizer was set to 873 K during the field measurements and calibration measurements. A collection efficiency of 0.74 was used for determination of chemical species concentrations; this value was determined from comparison between sulfate concentrations measured by means of AMS and non-sea-salt sulfate concentrations determined by means of total suspended particulate filter sample analysis during the field study in December 2010 (Irei et al., 2014). The detection limits (DLs) of the mass spectrometer for chloride, nitrate, ammonium, sulfate, organics, m/z 43 (an indicator for detection of hydrocarbon and aldehyde), and m/z 44 (an indicator for detection of carboxylic acid) were determined

by $3 \times$ standard deviation (SD) of blank concentrations obtained by measuring filtered ambient air (HEPA Capsule, Pall Corp.) for 2–16 h. The blank measurements were conducted every month during the study period. The average DLs of these species were 0.02, 0.04, 0.2, 0.4, 0.5, 0.02, and $0.06 \mu\text{g m}^{-3}$, respectively.

Mixing ratios for NO_x and NO_y were measured in situ to retrieve the $t[\text{OH}]$, an indicator of atmospheric oxidation. Measurement methods for NO_x and NO_y mixing ratios were developed with an LED converter and a molybdenum converter, respectively, together with commercially available NO_x analyzers (model 42 i-TL, Thermo Scientific). These instruments are described in detail elsewhere (Sadanaga et al., 2010; Yuba et al., 2010). DLs for NO , NO_2 , and NO_y were about 0.06 ppbv with 1 min averaging time. Mixing ratios of CO and O_3 were measured in situ with a CO analyzer (model 48, Thermo Scientific) and an O_3 analyzer (Model 49i, Thermo Scientific), respectively. The DLs of these instruments were 10 and 5 ppbv with 10 and 1 min averaging time, respectively. The analog signal output for these trace gas species was recorded every second using a data logger (NR-1000, KEYENCE), and hourly average mixing ratios were used for data analysis. Selected NMHCs (ethyne, *i*-pentane, and toluene) were also measured hourly with a gas chromatograph equipped with a flame ionization detector (6890N, Agilent Technologies) and coupled with an automated cryo-preconcentration sampler (Yokouchi, 2008). Ethyne, *i*-pentane, and toluene were chosen because those can be used as markers for vehicular emissions (Tang et al., 2009; Wang et al., 2015). The choice of toluene was also due to one of the possible precursors of atmospheric SOA (Grosjean and Seinfeld, 1989; Seinfeld and Pandis, 1999). The volatile organic compounds in 600 mL of ambient air were collected cryogenically from the main stream of the previously referred sampling line at a flow rate of 40 mL min^{-1} (i.e., a 15 min sampling period for a single measurement). Target compounds were identified and quantified on the basis of comparison with retention times and peak area counts for standards; specifically, a standard gas containing 1 ppb of each target compound was analyzed once a day. The DLs for ethyne, *i*-pentane, and toluene were 2.5, 1.5, and 1.5 pptv, respectively.

Additionally, ambient temperature, relative humidity (RH), precipitation, and wind speed and direction were measured with a weather transmitter (WXT 520, VAISALA, Helsinki, Finland).

3 Results and discussion

3.1 Meteorological observations

Measured ambient temperature ranged from 274.6 to 301.2 K, the mean \pm SD = $286.6 \pm 5.4 \text{ K}$ (Fig. S1). Ambient temperature showed a clear seasonal variation, and a polyno-

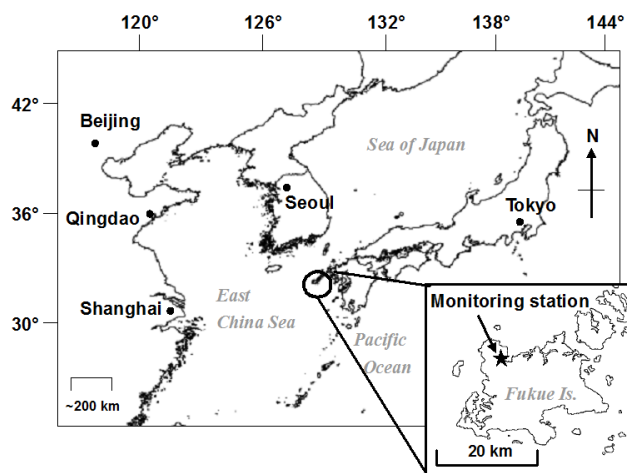


Figure 1. Location of the Fukue Island monitoring station.

mial best fit curve $\pm 5 \text{ K}$ covered $\sim 90\%$ of the data points and reproduced the observed trend.

Precipitation events were observed occasionally (Fig. S1), but their frequency and strength did not seem to significantly affect our overall interpretation of the entire data set. Therefore, in the analyses described hereafter, we included the data collected during the precipitation events, unless otherwise noted. RH varied between 25 and 100 % and seemed to be relatively constant from December to February and to vary more widely from March to May (Fig. S1).

A polar plot of hourly average wind speed shows that it ranged from 0.2 to 10 m s^{-1} (Fig. S2). The mean \pm SD of wind speeds during the observation period was $3 \pm 1 \text{ m s}^{-1}$, and the 90th, 25th, and 10th percentile cutoff values were 4, 2, and 1 m s^{-1} , respectively. This information suggests that medium-strength winds (i.e., wind speeds of $2\text{--}4 \text{ m s}^{-1}$) blew most of the time during the study period. Because wind directions measured at wind speeds of $< 1 \text{ m s}^{-1}$ are often treated as invalid, the fact that the 10th percentile cutoff for our data was 1 m s^{-1} indicates that 90 % of our wind direction data were valid. The most prevalent wind directions were between northwesterly and northeasterly (35 %) and between northeasterly and southeasterly (26 %). The prevalence of wind from the residential area of the peninsula (from the direction between southeasterly and southwesterly) was about 17 %.

3.2 Chemical species concentrations

The results of statistical analysis of the concentrations of chemical species in fine PM are summarized in Table 1, along with the results for gas-phase species. Because sea-salt PM tends to be coarse, the very low concentrations of chloride measured by means of AMS indicate that most of the chloride originating from sea salt was eliminated at the AMS inlet, which selects for fine PM. The mean concentrations \pm SDs of the chemical species in fine PM were similar

Table 1. Concentrations and mixing ratios of chemical species observed during the study period.

	Number of data	Mean	SD	Min ^a	Max	Lower quartile	Median	Upper quartile
Fine PM		(μg m ⁻³)						
Chloride	22 726	0.08	0.12	LDL	2.65	0.03	0.04	0.09
Ammonium		1.5	1.6	LDL	14.7	0.6	1.1	1.8
Nitrate		0.69	1.43	LDL	22.00	0.12	0.25	0.63
Sulfate		4.2	3.3	LDL	23.8	2.0	3.4	5.5
Organics		2.7	1.9	LDL	24.5	1.4	2.2	3.4
Total ^b		9.2	7.4	0.02	66.7	4.7	7.5	11.2
<i>m/z</i> 43 in organics		0.18	0.14	LDL	4.17	0.08	0.14	0.22
<i>m/z</i> 44 in organics		0.40	0.30	0.06	2.45	0.20	0.33	0.50
<i>m/z</i> 57 in organics		0.03	0.04	0.01	1.87	0.02	0.03	0.04
Gas-phase species		(ppbv)						
CO	4163	230	102	57	1136	160	204	272
NO	4176	0.06	0.16	LDL	4.45	LDL	LDL	0.06
NO _x	4176	1.39	1.16	LDL	12.70	0.70	1.10	1.70
NO _y	4163	4.86	3.49	0.13	25.41	2.49	3.95	6.03
O ₃	4165	45	11	10	97	38	45	52
<i>i</i> -Pentane	3856	0.106	0.079	LDL	2.055	0.066	0.098	0.132
Toluene	3856	0.110	0.142	LDL	2.625	0.044	0.071	0.123
Ethyne	3856	0.496	0.326	0.014	4.442	0.304	0.407	0.597

^a LDL: lower than detection limit.^b Sum of chloride, ammonium, nitrate, sulfate, and organics.

to those observed in 2003 at the same location (Takami et al., 2005) and at Cape Hedo, Okinawa (Takami et al., 2007). Sulfate was the predominant chemical species in fine PM throughout the observation period, accounting for 46 % on average, and was followed by organics (29 %), ammonium (16 %), and nitrate (8.0 %). The concentrations of nitrate, the detection of which is often an indication of the proximity of its emission source, were high in this study even though the monitoring station was located in a rural area. In many cases, the amount of nitrate in fine PM decreases or shifts to larger PM during long-range transport (Takiguchi et al., 2008, and references therein). Because there are no large emission sources of primary nitrate around the monitoring station, the high nitrate concentrations probably indicate mid- or long-range transport of pollutants from locations off the island. Temporal variation of the concentrations of organics in fine PM measured by means of AMS showed no seasonal trend, but some high-concentration episodes were observed (Fig. S3). It was also found that the concentrations of organic aerosols in the study period from 6 to 16 December, which was previously reported (Irei et al., 2014), were relatively low. In the time-series plot, the f_{44} , the fraction of m/z 44 in the organic mass spectrum or the fraction of carboxylate in organic aerosol, seemed to rise from ~ 0.12 to ~ 0.15 around the end of March. This increase may have been due to greater production of oxygenated organic compounds in spring than in winter because of the increasing sunlight irradiance in the spring, which was indicated by the times-series plot of ambient temperature (Fig. S1).

Most of the O₃ mixing ratios were < 55 ppbv, and the mean of 45 ppbv was consistent with the annual mean of ~ 50 ppbv observed at the same location in 2011 (Kanaya et al., 2016); this annual mean of ~ 50 ppbv was the lowest annual mean O₃ mixing ratio observed over the course of 6 years (2009–2014) at this location. A times-series plot of hourly average O₃ mixing ratios showed that although there were some episodes of high mixing ratios, the mixing ratios seemed to vary between ~ 25 and ~ 50 ppbv from December to February and then were prone to gradually increase from the beginning of March to May (Fig. S4a). Similar seasonal trends have been observed at the same location (Kanaya et al., 2016) and at other remote sites in East Asia (Pochanart et al., 2002; Suthawaree et al., 2008; Kanaya et al., 2016, references therein). This trend was similar to the f_{44} trend described above and therefore can also be explained in terms of an increase in sunlight irradiance to polluted air masses transported from the Asian continent. Meanwhile, according to the observations at the other remote sites referred above, the O₃ mixing ratios tend to drop starting in May and continuing into the summer because the origin of air masses changes from the continent directly to the Pacific Ocean; the oceanic air masses generally contain much lower quantities of O₃ and its precursors. The drop in the O₃ mixing ratios observed between 9 and 12 May was compatible with the influence of the oceanic air masses demonstrated by the back trajectories

of air masses (Fig. S5) modeled by HYSPLIT (Draxler and Rolph, 2013).

The NO_x mixing ratios ranged from lower than the DL (LDL, <0.006 ppbv) to 12.70 ppbv (mean \pm SD = 1.39 ± 1.16 ppbv), and the NO_y mixing ratios ranged from 0.13 to 25.41 ppbv (mean \pm SD = 4.86 ± 3.49 ppbv). The upper quartile cutoffs for these mixing ratios were 1.70 and 6.03 ppbv, respectively. NO was found to be the very minor component of NO_x . The median and lower and upper quartile cutoff values of NO were LDL, LDL, and 0.06 ppbv, respectively. Compared to the mixing ratios observed in other field studies (Pandey Deolal et al., 2012, and references therein), most of these mixing ratios fell between those observed at European rural and background sites. No time-dependent trend was observed for the NO_x or NO_y mixing ratio (Fig. S4b, c). Episodes of high mixing ratios were observed irregularly.

The CO mixing ratios ranged from 57 to 1136 ppbv, and the median, upper, and lower quartile cutoff values were 204, 272, and 160 ppbv, respectively; no seasonal trend was observed (Fig. S4d). Except for some episodes of high mixing ratios, the observed mixing ratios below the upper quartile cutoff seem to be comparable in magnitude to those observed from 2002 to 2005 at various rural and remote locations in the region of the East China Sea (Suthawaree et al., 2008; Tanimoto et al., 2008), indicating that the mixing ratios we observed reflected the background mixing ratios in this region. A polar plot of the wind-sector dependence of the CO mixing ratio showed almost no sharp increases attributable to local anthropogenic emissions (Fig. S6). The episodes of high mixing ratios that occurred at irregular intervals were attributed to mid-range transport of anthropogenic emissions.

To determine whether these episodes were due to combustion-related pollution transported from the Asian continent, we chose seven time periods with high CO mixing ratios that lasted for more than 24 h, and we checked the back trajectories of the air masses modeled by HYSPLIT. These episodes are listed in Table S1, together with confirmation of concentration rises of other chemical species during the high-CO episodes. Back trajectories for each episode showed that the air masses were transported from the region of east coast of China or of west coast of Korea during these episodes. The trajectories also showed that the episodes ended with the arrival of air masses from the Pacific Ocean or Mongolia with greater wind speed (Figs. S7 to S13). Thus, these results roughly support the proposition that at least these seven high-concentration episodes were derived from the Asian continent.

Most of the observed mixing ratios for *i*-pentane, toluene, and ethyne (Table 1) were slightly higher than the ratios observed at Cape Hedo, Okinawa, in 2000 (Kato et al., 2004). This result is consistent with the fact that pollutants transported from the Asian continent to Fukue are often fresher than those transported to Cape Hedo (Takami et al., 2007). Times-series plots of the mixing ratios for these NMHCs

showed no seasonal trends (Fig. S4e–g). The observed sharp rises in mixing ratios of *i*-pentane, toluene, and ethyne – which lasted no more than a few hours, indicating the influence of anthropogenic emissions near the site – accounted for only a small portion of the observed data.

3.3 Correlations between the concentrations of various chemical species

Investigation of the correlations between the concentrations of various chemical species showed that CO concentration was correlated with the concentrations of NO_y ($r^2 = 0.674$), ethyne ($r^2 = 0.724$), and organic aerosols ($r^2 = 0.562$) (Table 2). Ethyne is a combustion marker and often originates from vehicular emission, which is one of the major sources of NO_x as well. The atmospheric lifetimes of CO and ethyne are usually determined by the reactions with OH radicals (the most powerful oxidant in the air). Under an average OH concentration of 5×10^5 molecules cm^{-3} , which is the calculated diurnally averaged OH concentration during the PEACE-A aircraft campaign over Japan in January 2002 (Takegawa et al., 2004), their lifetimes are approximately 100 and 35 days, respectively. Meanwhile, they observed very high correlation between NO_y and CO (or CO_2) and found that the lifetime of NO_y during the long-range transport of NO_y from the Asian continent to Japan was 1.3–2.0 days, which was mainly due to the wet and/or dry depositions of HNO_3 . That is, $\sim 60\%$ of NO_y sinks within 2.0 days. This sink is likely due to the dry deposition because of the constant life time over the six different flight studies at various altitudes (0.2–4.0 km): if the sink were due to the wet deposition, the larger variation in the NO_y lifetime should have been observed. We expect that the order of NO_y lifetime in our study is similar because the dry deposition was likely the major sink of NO_y during our study and also because the transport time of transboundary air pollutants during our study was similar. The slope of the linear regression drawn for the NO_y mixing ratio as a function of CO mixing ratio was approximately 0.03, which is on the similar order of the value of ~ 0.038 observed by Takegawa et al. (2004) in the 2–3-day aged plume originated from Japan. The slope also coincided with the calculated NO_y / CO ratio of 0.03 in an air mass transported a long distance from its origin to Korea using a recent emission inventory (Kim et al., 2012). In contrast, NO_x to CO ratios at emission are generally higher than those values (Parrish et al., 2002). Kurokawa et al. (2013) reported that emission ratios of NO_x to CO from coal combustion used in industry in China, which is suspected to be one of the major sources of these pollutants observed in our study, were 0.06–0.07. With consideration of the NO_y lifetime by the depositions and of the transport time of roughly 1–3 days estimated by the back trajectories previously referred, the discrepancy between the NO_y / CO observed at Fukue and the NO_x / CO at emission seems to be reasonably explained by the depositional sink during the transport. The

Table 2. Coefficients of determination for correlations between chemical species concentrations.

	PM_NH ₄	PM_NO ₃	PM_SO ₄	PM_org	<i>m/z</i> 43	<i>m/z</i> 44	<i>m/z</i> 57	O ₃	NO _x	NO _y	CO	<i>i</i> -Pentane	Toluene	Ethyne
PM_NH ₄	1	0.693	0.639	0.696	0.443	0.755	0.323	0.251	0.007	0.480	0.405	0.004	0.026	0.097
PM_NO ₃	0.693	1	0.263	0.529	0.389	0.521	0.320	0.145	0.035	0.544	0.314	0.025	0.051	0.107
PM_SO ₄	0.639	0.263	1	0.430	0.380	0.463	0.191	0.128	0.001	0.179	0.371	0.013	0.006	0.125
PM_org	0.696	0.529	0.430	1	0.747	0.949	0.606	0.303	0.053	0.559	0.562	0.060	0.081	0.198
<i>m/z</i> 43	0.443	0.389	0.380	0.747	1	0.640	0.588	0.146	0.153	0.459	0.543	0.100	0.094	0.301
<i>m/z</i> 44	0.755	0.521	0.463	0.949	0.640	1	0.471	0.384	0.016	0.510	0.526	0.007	0.039	0.142
<i>m/z</i> 57	0.323	0.320	0.191	0.606	0.588	0.471	1	0.098	0.160	0.417	0.394	0.106	0.137	0.236
O ₃	0.251	0.145	0.128	0.303	0.146	0.384	0.098	1	0.007	0.292	0.288	0.013	0.006	0.053
NO _x	0.007	0.035	0.001	0.053	0.153	0.016	0.160	0.007	1	0.309	0.136	0.195	0.225	0.221
NO _y	0.480	0.544	0.179	0.559	0.459	0.510	0.417	0.292	0.309	1	0.674	0.117	0.155	0.422
CO	0.405	0.314	0.371	0.562	0.543	0.526	0.394	0.288	0.136	0.674	1	0.193	0.126	0.724
<i>i</i> -Pentane	0.004	0.025	0.013	0.060	0.100	0.007	0.106	0.013	0.195	0.117	0.193	1	0.410	0.435
Toluene	0.026	0.051	0.006	0.081	0.094	0.039	0.137	0.006	0.225	0.155	0.126	0.410	1	0.302
Ethyne	0.097	0.107	0.125	0.198	0.301	0.142	0.236	0.053	0.221	0.422	0.724	0.435	0.302	1

higher coefficient of determination between CO and ethyne than that between CO and NO_y also supports the association of their correlation with their lifetimes. Despite such significant depositional loss of NO_y, the positive correlation with the r^2 of 0.674 between CO and NO_y implies that the wet deposition, which is highly variable and influential, did not significantly contribute to the NO_y sink; in turn, the major sink of NO_y was the dry deposition depending on the gravitational residence time.

Particulate ammonium was correlated with particulate acidic components, such as sulfate, nitrate, organics, and *m/z* 44 of organics. The highest correlation with *m/z* 44 ($r^2 = 0.755$) suggests that the organics were primarily composed of carboxylic acids. The observed correlations imply that sufficient amount of ammonium was available in the gas phase to neutralize all these acidic components. Although it is not shown, slopes of linear regressions between ammonium (x axis) and sulfate, nitrate, or organics (y axis) were 1.7, 0.74, and 1.0, respectively. With respect to molar ratio to ammonium, sulfate and nitrate were calculated to be 0.32 and 0.21, respectively. If only sulfate and nitrate were neutralized by ammonium, the sum of the nitrate molar ratio and 2 times the sulfate molar ratio must be equivalent to 1. The actual number for the sum is 0.85, lower than the neutralization ratio. This suggests that the amount of ammonium in PM_{1.0} was more than enough to neutralize sulfate and nitrate. Because organics were more highly correlated with ammonium than with sulfate and nitrate (Table 2), it is possible to conclude that the excess amount of ammonium was to neutralize organic acid. Given that all three acidic species were neutralized by ammonium, the molar ratio of organic acid to ammonium accounts for 0.15. As the number of carboxylic group in the organic acid molecule is referred to as n , the organic acid molar ratio allows us to estimate the average molecular weight of organic acid as $120 \times n \text{ g mol}^{-1}$.

The overall correlation between *m/z* 43 and *m/z* 44 in the organic mass spectra obtained by AMS was 0.640, but a plot of *m/z* 43 versus *m/z* 44 showed two distinct trends: a

trend with an *m/z* 44 to *m/z* 43 ratio of ~ 2.5 and another with a ratio of ~ 1 (Fig. S14), the latter of which was clearly observed in the period from the end of December to the beginning of February. These results suggest that two types of organic species gave fragment ions that contributed to the *m/z* 44 to *m/z* 43 ratio. These species will be discussed in detail in Sect. 3.4.

3.4 Oxidation state of organic aerosols

As we did in previous reports for the field studies in December 2010 (Irei et al., 2014) and in March 2012 (Irei et al., 2015), here we briefly discuss the results of evaluation of the oxidation state of the organic aerosols observed during the half-year period of this study. First, we applied positive matrix factorization (PMF) analysis to the organic aerosol mass spectra to deconvolute the types of organic aerosols (Zhang et al., 2005; Ulbrich et al., 2009), and then we determined the oxidation state of each type of organic aerosol by plotting the fractions of *m/z* 43 (f_{43}) and *m/z* 44 (f_{44}) in the organic mass spectra, according to the method described by Ng et al. (2010). Furthermore, we determined the mass to carbon ratios (OM/OC ratios) of the types of organic aerosol using the method described by Zhang et al. (2005) to characterize the species of the organic aerosols.

With respect to the mass spectral pattern, PMF analysis on the whole data set of organic mass spectra gave the most feasible solution with two types of organic aerosols (Fig. 2). The mass spectral patterns of these two types of aerosols agreed well with those of hydrocarbon-like organic aerosol (HOA) and low-volatility oxygenated organic aerosol (LV-OOA) found in the December study (r^2 of 0.98 and 0.98, respectively). The patterns also agreed reasonably with the reference mass spectra for LV-OOA and HOA in the AMS spectral database (r^2 of 0.94 and 0.53, respectively) made available by Ulbrich et al. (2015) (<http://cires.colorado.edu/jimenez-group/AMSsd/>). For the identification of HOA, the negligibly small intensity at *m/z* 44 with the high intensity at *m/z* 43 in the mass spectra was crucial to differentiate

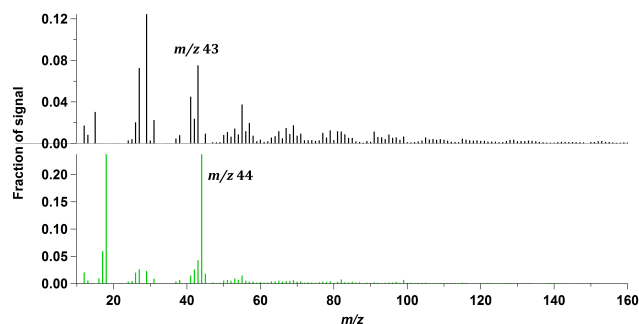


Figure 2. Extracted mass spectra from two-factorial PMF analysis: (top) mass spectra identified as HOA; (bottom) mass spectra identified as LV-OOA.

from the mass spectra for semi-volatile oxygenated organic aerosol (SV-OOA). However, the detailed analysis exhibited that PMF analysis on smaller data set sometimes gives mass spectra patterns identified as LV-OOA and SV-OOA, the latter of which has a high signal at m/z 43 and marginally high signal at m/z 44 (e.g., $f_{43} = 0.058$ and $f_{44} = 0.022$ shown in Fig. S15). Thus, it is worth noting that, due to the large data set, the overall PMF analysis here may have not separated a SV-OOA loading from a HOA loading successfully. The time-series variations of the HOA and LV-OOA mass concentrations showed similar patterns (Fig. 3), an implication that the primary OA and the precursor(s) of LV-OOA are possibly from the same source on a large scale. On average, HOA and LV-OOA accounted for 38 and 59 % of the organic aerosols throughout the study period, respectively. These values are in the same magnitude to the fractions previously reported during the study in December 2010 (32 and 67 % for HOA and LV-OOA, respectively). In a plot of f_{43} versus f_{44} , the data point of f_{43} and f_{44} for LV-OOA (0.043 and 0.237, respectively) in this study was located at the top of the triangle, indicating a high oxidation state (Fig. 4). Meanwhile, the data point of f_{43} and f_{44} for HOA (0.075 and 0, respectively) was located at the bottom of the triangle, indicating a low oxidation state. The f_{44}/f_{43} ratios for LV-OOA and HOA were approximately 5 and 0, respectively. The ratio for LV-OOA was 2 times the high slope in the plot of m/z 44 versus m/z 43 (~ 2.5) as referred in the previous section (Fig. S14), and the ratio for HOA was lower than the low slope (approximately 1). According to the results of the overall PMF analysis, the observations shown in Fig. S14 could be explained by a combination of HOA (or SV-OOA) and LV-OOA. The OM / OC ratio of HOA and LV-OOA were 1.7 and $4.2 \mu\text{g} \mu\text{gC}^{-1}$, respectively. The OM / OC ratio of HOA was similar to the ratio of HOA found in the December study, $1.2 \mu\text{g} \mu\text{gC}^{-1}$. The OM / OC ratio of LV-OOA was also similar to the ratios of LV-OOA found in our field studies in December 2010 ($3.6 \mu\text{g} \mu\text{gC}^{-1}$) and March 2012 ($4.3 \mu\text{g} \mu\text{gC}^{-1}$), respectively. Based on the AMS reference mass spectra available from the website previously

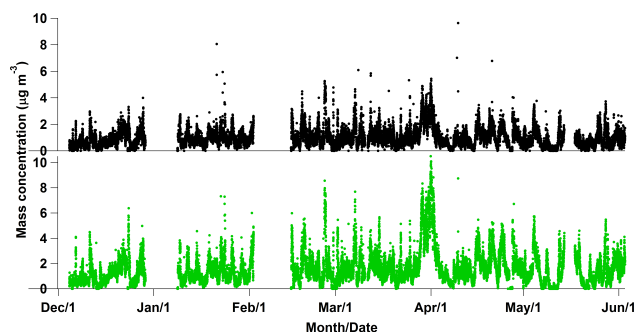


Figure 3. Temporal variation of mass concentration of HOA (orange) and LV-OOA (green) obtained by PMF analysis.

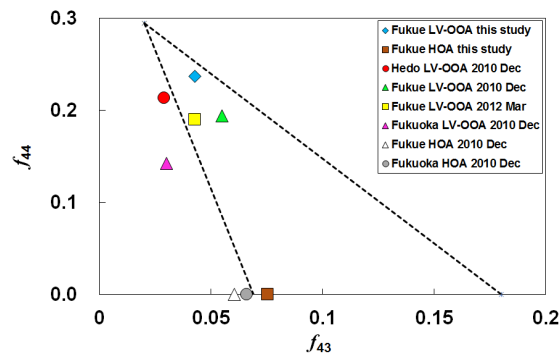


Figure 4. Plot of f_{44} versus f_{43} for different types of organic aerosols extracted from PMF analysis. Dashed lines are the limits of oxidation states reported by Ng et al. (2010).

referred, substances showing such a high OM / OC ratio are only humic-like substances.

3.5 Chemical clocks

We used a $\text{NO}_x / \text{NO}_y$ concentration ratio and a NMHC concentration ratio to explore the extent of photochemical reaction (i.e., the reaction with OH radical). In this type of chemical clock analysis, the concentration of a reactive chemical and that of a less reactive chemical are used in the numerator and the denominator, respectively, of the ratio. As a reaction proceeds, the numerator decreases while the denominator remains constant; therefore, a change in the ratio indicates the extent of reaction. In application of chemical clocks to the atmospheric transport of pollutants, users should be aware that the extent of reaction may not always be well defined because emission sources are spatially distributed over the trajectory of an air parcel in many cases. This type of analysis is ideally suited to situations in which inputs into an air parcel from additional emission sources during transport are negligible. Our field study for transboundary air pollution transported over the East China Sea can be the ideal case.

3.5.1 NO_x / NO_y clock

To see whether such an assumption is valid, the NO_x / NO_y and hydrocarbon clocks were evaluated. Given that the conversion of NO₂ (the major component of NO_x) to HNO₃ (one of the components of NO_y),



is the major sink for NO_x and that the concentration of OH radicals, [OH], can be assumed to be constant, the photochemical age, $t[\text{OH}]$, of NO_x can be determined according to the following pseudo-first-order rate law:

$$t[\text{OH}] = -\frac{1}{k_{\text{NO}_2}} \ln \frac{[\text{NO}_x]}{[\text{NO}_y]}, \quad (1)$$

where [NO_x], [NO_y], and k_{NO_2} are the concentrations of NO_x and NO_y (molecules cm⁻³) at reaction time t and the temperature-dependent effective second-order rate constant for the reaction of NO_x with OH radicals, respectively. k_{NO_2} includes the concentration of a third body, [M], which depends on pressure and temperature. To calculate k_{NO_2} at ambient temperature and a pressure of 1 atm, we therefore calculated the third-order rate constant and [M] according to the method described by Finlayson-Pitts and Pitts (2000) with the polynomial best fit for the measured ambient temperature mentioned in Sect. 3.1. The calculated k_{NO_2} values at 1 atm ranged from 9.3×10^{-12} to 1.1×10^{-11} cm³ molecule⁻¹ s⁻¹, and both the mean and median were 1.0×10^{-11} cm³ molecule⁻¹ s⁻¹. In turn, the determined $t[\text{OH}]$ using the k_{NO_2} values and the [NO_x] / [NO_y] ratios ranged from 2.9×10^5 to 1.3×10^8 (mean \pm SD = $(3.4 \pm 1.6) \times 10^7$ h molecules cm⁻³). We found that the use of a fixed k_{NO_2} value (i.e., the mean value of 1.0×10^{-11} cm³ molecule⁻¹ s⁻¹) resulted in biases between -10 and $+7$ % in the estimation of $t[\text{OH}]$. We also found that a temperature variation of ± 5 K resulted in only a ± 5 % variation in $t[\text{OH}]$. However, this analysis for the biases does not take into account temperature and pressure variations during the transport of the air parcels.

The reaction of NO₂ with O₃, which may result in significant overestimation in the NO_x / NO_y clock, was also evaluated. The reaction of NO₂ with O₃ forms NO₃ radicals:



This reaction channel is important at night but negligible during the day when NO₃ radicals are quickly photolyzed back to NO_x. NO₃ radicals react with NO₂ to form stable N₂O₅, which is in thermal equilibrium with NO₂ and NO₃ and therefore acts as a reservoir of NO_x:

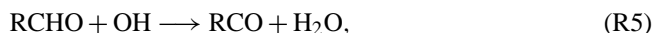


N₂O₅ reacts slowly with water to form HNO₃, and this process terminates the chain reaction:



The (R4) channel is known to be predominant at the surface of particles (Brown et al., 2006). Although the nocturnal sink of NO_x by the series of (R2)–(R4) channels may result in a significant overestimation of $t[\text{OH}]$, the heterogeneous uptake of N₂O₅ (i.e., the (R4) channel) is negligible when a sufficient amount of nitrate already exists in particles because the preexisting nitrate inhibits the forward reaction of (R4) channel (Brown et al., 2006). We have observed that there was enough ammonium that neutralized sulfate and nitrate. Therefore, the negligibly small heterogeneous uptake of N₂O₅ is likely our case. Indeed, a plot of the hourly O₃ mixing ratios (x axis) versus hourly $\ln([\text{NO}_x] / [\text{NO}_y])$ (y axis) showed no positive correlation but a clear inverse correlation ($r^2 = 0.489$), indicating that the turnover of NO_x to NO_y increased as the O₃ mixing ratio increased (Fig. 5). If the reaction of NO₂ with O₃ and the subsequent reactions were the predominant mode of conversion of NO_x to NO_y at night, a positive correlation between the O₃ mixing ratio and the extent of NO_x turnover – that is, between the O₃ mixing ratio and $\ln([\text{NO}_x] / [\text{NO}_y])$ – should be observed in our nighttime data. Similar observations have been reported elsewhere (Olszyna et al., 1994; Roussel et al., 1996). Given that during the day, O₃ forms only photochemically, this inverse correlation suggests that NO_x conversion was due to daytime photochemistry. A conclusion with this possibility was drawn from an analysis of O₃ production efficiency (Yokouchi et al., 2011).

The photochemical reaction of aldehydes is also a sink for NO₂, resulting in the formation of thermally stable peroxyacyl nitrates:



Unfortunately, we cannot evaluate the significance of this channel with our current data set, because no data for aldehyde and peroxyacyl radical concentrations are available. Because this loss channel also occurs in sunlight, the possibility that peroxyacyl nitrate formation significantly affects $t[\text{OH}]$ cannot be excluded. The absolute value of $t[\text{OH}]$ derived from the [NO_x] / [NO_y] ratio remains uncertain, but as demonstrated by the high correlation between this ratio and the O₃ mixing ratio, the use of the NO_x / NO_y clock nevertheless provides valuable information about the relative extent of photooxidation. When we plotted the time-series variation of $t[\text{OH}]$ estimated from the [NO_x] / [NO_y] ratio (Fig. 6), we observed variation similar to that observed for the hourly average O₃ mixing ratio (Fig. S4a), implying a strong association between the $t[\text{OH}]$ and the sunlight irradiance.

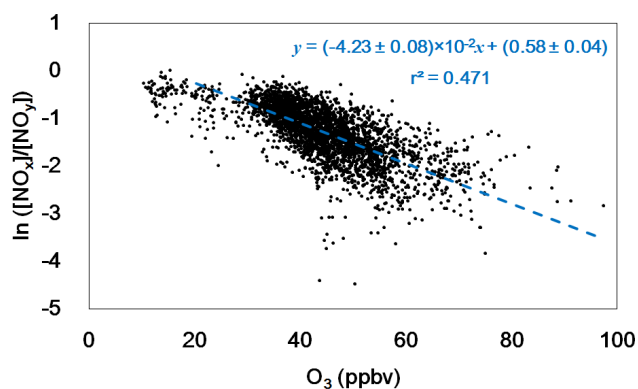
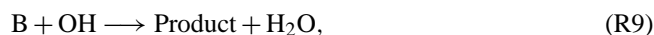
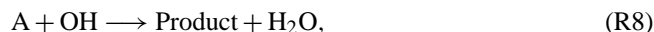


Figure 5. Scatter plot of natural logarithm of $[\text{NO}_x]/[\text{NO}_y]$ ratio versus O_3 mixing ratio. The data points with the ozone mixing ratios less than 25 ppbv were excluded from the linear regression.

3.5.2 Hydrocarbon clock

When NMHC A and B react with OH radicals at different rates,



$t[\text{OH}]$ can also be estimated from the ratio of the two NMHCs (Roberts et al., 1984; Rudolph and Johnen, 1990; Parrish et al., 1992):

$$t[\text{OH}] = \frac{1}{(k_A - k_B)} \ln \left(\frac{[\text{A}_0]}{[\text{B}_0]} \cdot \frac{[\text{B}]}{[\text{A}]} \right), \quad (2)$$

where $[\text{A}_0]$ and $[\text{B}_0]$ are the initial concentrations (molecules cm^{-3}) of NMHCs A and B, which have short and long lifetimes (relative to each other); $[\text{A}]$ and $[\text{B}]$ are the concentrations (molecules cm^{-3}) at time t ; and k_A and k_B are the temperature-dependent rate constants for reactions of A and B with OH radicals ($\text{molecules}^{-1} \text{cm}^3 \text{s}^{-1}$). If NMHCs A and B are emitted from the same source at the same time, the change in the concentration ratio theoretically indicates the extent of chemical reaction. However, dilution with an aged air mass containing depleted NMHCs can also change the NMHC ratio, thus biasing the $t[\text{OH}]$ estimation (McKeen and Liu, 1993). This bias can be visualized by plotting two different NMHC ratios with the same denominator, and we used the $[i\text{-pentane}]/[\text{ethyne}]$ and $[\text{toluene}]/[\text{ethyne}]$ ratios for this evaluation. The calculations require the rate constants for the reactions of the NMHCs with OH radicals at the mean temperature observed, 283.7 K, the mixing ratios of the NMHCs in the background air, and their initial mixing ratios at emission. Using the Arrhenius equation with the recommended parameters for *i*-pentane, toluene, and ethyne (NIST Chemistry WebBook, <http://webbook.nist.gov/chemistry/>), the rate constants for the reaction of these compounds with OH radicals

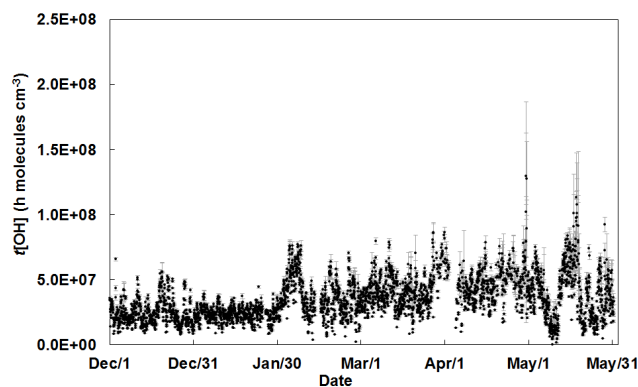


Figure 6. Time-series variation of photochemical age, $t[\text{OH}]$, estimated from $[\text{NO}_x]/[\text{NO}_y]$ ratios.

at 283 K (i.e., the mean temperature during the study period) were calculated to be 3.44×10^{-12} , 5.88×10^{-12} , and $7.38 \times 10^{-13} \text{ cm}^3 \text{ molecule}^{-1} \text{ s}^{-1}$, respectively. Note that the variation of the slope for the reaction loss due to the variation of the temperature-dependent rate constants between the maximum and minimum temperature (298.3 and 271.5 K) was found to be less than $\pm 2\%$. Thus, the variation of the reactive loss due to the temperature change was not influential to our analysis. For the background mixing ratios, we used mixing ratios observed at Cape Hedo, Okinawa (Kato et al., 2004), which were 0.05, 0.09, and 0.39 ppbv, respectively. For the initial mixing ratios at emission, we used the reported scores for loadings extracted by means of PMF analysis for the NMHC sources in Beijing (Wang et al., 2015). The PMF loadings used in the calculations were vehicular emissions 1 and 2, solvent use, and natural gas and gasoline leakage. In addition to these initial mixing ratios, mixing ratios reported at a rural site in northeastern China (Lin'an, in the Yangtze River Delta, Tang et al., 2009) were also tested.

The plot shows that, with respect to the initial NMHC ratio, depletion trends resulting from use of the solvent-use profile and of the observations in Lin'an deviated substantially from the observed overall trend (Fig. 7). The majority of observed plots lies between the trends for the dilution with the background air and the reaction loss calculated if the profiles for the vehicular emissions and natural gas and gasoline leakage were used. That is, the vehicular emissions and the natural gas and gasoline leakage may have been the predominant emitters of these NMHCs, but source apportionment is difficult because of the uncertainty in the emission profiles. On the basis of this comparison, we could identify only two possible significant sources of these NMHCs during the measurement period. The layout of observed data points between the dilution and reactive loss lines also suggests that depletion in their mixing ratios was a combination of these processes. Comparison of calculated $t[\text{OH}]$ by the toluene/ethyne clock with those by the NO_x/NO_y clock exhibited a poor correlation (Fig. S16), demonstrating

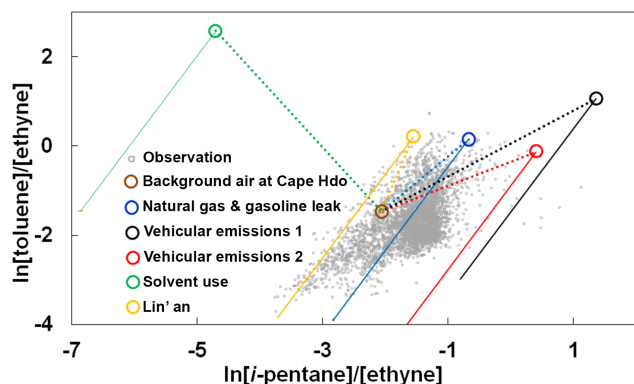


Figure 7. Scatter plot of natural logarithm of [toluene]/[ethyne] ratio as a function of natural logarithm of [i-pentane]/[ethyne] ratio (gray dots). Linear regressions shown are calculated depletion trends resulting from mixing with background air (dotted lines) and from reaction with OH radicals (solid lines); these trends were determined by using the initial NMHC ratios from the literature, for vehicular emissions 1 (black open circle), vehicular emissions 2 (red open circle), solvent use (green open circle), and natural gas and gasoline leakage (blue open circle) observed in Beijing (Wang et al., 2015), as well as field measurement data obtained at Lin'an, a rural background site in the Yangtze River Delta, China (yellow open circle), from Tang et al. (2009). The brown open circle that all the dotted lines meet at corresponds to the background values observed at Cape Hedo (Kato et al., 2004). See the text for the calculation and references for these data.

the limitation of the toluene/ethyne clock for estimation of $t[\text{OH}]$ under the condition at Fukue. A quantitative understanding will require a more sophisticated analysis based on mass balance with reliable source profiles.

With respect to the background mixing ratios observed at Cape Hedo, the plot also shows that many of our observed data points were lower than the background NMHC ratios represented by a brown circle in Fig. 7. This result implies that the background NMHC ratios from the observations at Cape Hedo are still too high to be used as background values of these NMHC ratios for the study region. It is reasonable to assume that the background mixing ratios for both toluene and *i*-pentane in the aged air masses were LDL (< 3 pptv). This assumption allows us to approximate the background mixing ratio of ethyne based on the smallest [toluene]/[ethyne] and [i-pentane]/[ethyne] ratios observed. According to the plot, the use of -3.5 for the $\ln[\text{toluene}]/[\text{ethyne}]$ and -4 for $\ln[\text{i-pentane}]/[\text{ethyne}]$, approximately the smallest ratios observed, seems more reasonable. If we use the highest DL value (3 pptv) as the background mixing ratio for toluene and *i*-pentane, the background ethyne mixing ratio is then calculated to be ~ 0.16 ppbv, which is about 25 % of the background value observed at Cape Hedo by Kato et al. (2004). On the basis of the plot in Fig. 7, we recommend the use of 0.003, 0.003, and 0.16 ppbv as the background mixing ratios for *i*-pentane,

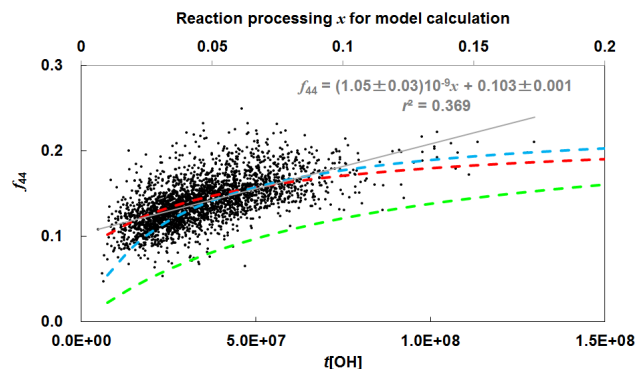


Figure 8. Scatter plot of hourly averaged f_{44} (black dot) as a function of photochemical age, $t[\text{OH}]$, estimated by means of the NO_x/NO_y clock (the bottom x axis) and a linear regression (gray line). As comparison, f_{44} binary mixing models (dotted curves) of HOA and LV-OOA using different combinations of model parameters (combination I (green), combination II (blue), and combination III (red)) are also shown. See the text for the detail of the combinations of model parameters.

toluene, and ethyne, respectively, in the region of the East China Sea.

3.6 Dependence of f_{44} and O_3 on $t[\text{OH}]$

A scatter plot of f_{44} as a function of $t[\text{OH}]$ estimated by the NO_x/NO_y clock showed a proportional increase of f_{44} with increasing $t[\text{OH}]$ (estimated by means of the NO_x/NO_y clock) up to a $t[\text{OH}]$ value of 7×10^7 h molecules cm^{-3} , and then f_{44} started to level off slightly (Fig. 8). That is, f_{44} works as an oxidation indicator below the $t[\text{OH}]$ of 7×10^7 h molecules cm^{-3} . The f_{44} oxidation indicator is known to be case dependent, even at this location and below this upper limit (Irei et al., 2015). Considering the existence of HOA during the study period, a series of findings here and in the previous reports supports our hypothesis that f_{44} varies with $t[\text{OH}]$ as LV-OOA, which has a constant and high value of f_{44} , mixes with the background-level HOA, which has a significantly lower constant value of f_{44} than LV-OOA (Irei et al., 2014). To a first approximation of the increasing trend, f_{44} is given by

$$f_{44} = (1.05 \pm 0.03) \times 10^{-9} t[\text{OH}] + 0.103 \pm 0.001, \quad (3)$$

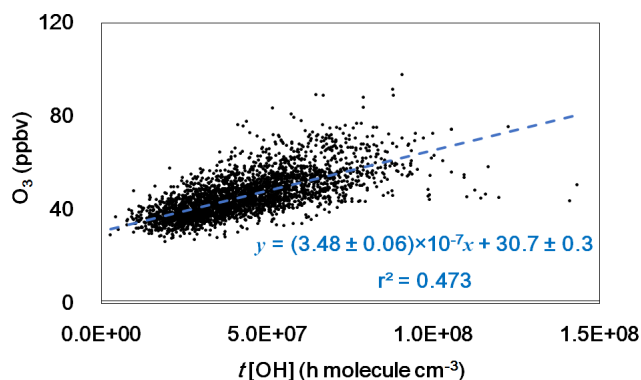
with an r^2 value of 0.369. The first approximation satisfactorily describes the increasing trend below a $t[\text{OH}]$ value of 7×10^7 h molecules cm^{-3} . The intercept of the first approximation indicates the f_{44} value for organic aerosol at a photochemical age of zero, that is, f_{44} at emission. The slope, which was $(1.05 \pm 0.03) \times 10^{-9} \text{ h}^{-1} \text{ molecule}^{-1} \text{ cm}^3$, indicates the rate of increase of f_{44} as $[\text{OH}]$ is given. Kleinman et al. (2007) observed that during the New England Air Quality Study, the background-corrected f_{44} value increased from 0.08 to 0.13 as $-\ln([\text{NO}_x]/[\text{NO}_y])$ increased

Table 3. Three different combinations of model parameters.

Parameters	Combination I ^a	Combination II ^a	Combination III ^b
a ($\mu\text{gC m}^{-3}$)	0.05	0.025	0.05
b ($\mu\text{gC m}^{-3}$)	1	1	1
HOA f_{44}	0	0	0.08
LV-OOA f_{44}	0.237	0.237	0.22
(OM / OC) _{HOA} ($\mu\text{g } \mu\text{gC}^{-1}$)	1.7	1.7	1.2
(OM / OC) _{LV-OOA} ($\mu\text{g } \mu\text{gC}^{-1}$)	4.2	4.2	3.7

^a The f_{44} and OM / OC values for HOA and LV-OOA are based on the results from the PMF analysis.

^b Parameters used in the previous report (Irei et al., 2014, Supplement)

**Figure 9.** Scatter plot of ozone mixing ratio versus photochemical age ($t[\text{OH}]$). The data points with the ozone mixing ratios less than 25 ppbv were excluded from the linear regression.

from 0.1 to 1.3, which corresponds to an increase of $t[\text{OH}]$ from 3.2×10^6 to 42×10^6 $\text{h molecule cm}^{-3}$. These values give an increase rate of $1.3 \times 10^{-9} \times [\text{OH}] \text{ h}^{-1}$, which is almost identical to the rate we calculated in this study. The overall proportionality of f_{44} with $t[\text{OH}]$ suggests that, like the $\text{NO}_x / \text{NO}_y$ clock, f_{44} worked as an oxidation indicator during this study period. This, however, is inconsistent with our other report, in which no proportional increase of f_{44} was observed during the study in different year at the same location (Irei et al., 2015). Interestingly, our hypothesis of binary mixture of organic aerosol is still consistent with these contradicting cases.

It has been proposed that the increasing trend of f_{44} can be explained by a binary mixture of variable amount of LV-OOA depending on extent of reaction processing x for the LV-OOA precursor and constant amount of HOA (Irei et al., 2014, Supplement):

$$f_{44} = \frac{\text{HOA } f_{44} \cdot a \cdot \left(\frac{\text{OM}}{\text{OC}}\right)_{\text{HOA}} + \text{LV-OOA } f_{44} \cdot \left[0.3x \cdot b \cdot \left(\frac{\text{OM}}{\text{OC}}\right)_{\text{LV-OOA}}\right]}{a \cdot \left(\frac{\text{OM}}{\text{OC}}\right)_{\text{HOA}} + \left[0.3x \cdot b \cdot \left(\frac{\text{OM}}{\text{OC}}\right)_{\text{LV-OOA}}\right]} \quad (4)$$

In this equation $\text{HOA } f_{44}$ and $\text{LV-OOA } f_{44}$ are the fractions of m/z 44 signal for the HOA and LV-OOA factors from the PMF analysis previously discussed, respectively; $(\text{OM} / \text{OC})_{\text{HOA}}$ and $(\text{OM} / \text{OC})_{\text{LV-OOA}}$ are the organic mass concentration ratios to the organic carbon concentrations ($\mu\text{g } \mu\text{gC}^{-1}$) for the HOA and LV-OOA from the PMF analysis, respectively; and a and b values are arbitrary constants ($\mu\text{gC m}^{-3}$) that convert the $(\text{OM} / \text{OC})_{\text{HOA}}$ and $(\text{OM} / \text{OC})_{\text{LV-OOA}}$ ratios to the organic mass concentrations of the HOA and the LV-OOA, respectively. The factor “0.3”, which is multiplied by the variable x , is a factor for the SOA carbon yield based on the laboratory experiments of SOA formation by toluene photooxidation (Irei et al., 2006, 2011). Equation (4) has one variable, x , and six parameters, four of which are determined by PMF analysis. The greater extent of reaction proceeds, the greater LV-OOA contributes to the binary mixture of HOA and LV-OOA, each of which has significantly different f_{44} value. Consequently, the f_{44} of the binary mixture containing a significantly low f_{44} continues to increase until it is saturated with LV-OOA. This hypothesis consistently explains our observations that the f_{44} oxidation indicator sometimes worked and sometimes did not. There is also a possible limitation that the indicator also depends on distinctive values of f_{44} . If two members had the similar f_{44} values, the indicator would not work.

The f_{44} curve of organic aerosols was calculated using three different combinations of parameters listed in Table 3. It was found that the model calculation underestimated the f_{44} (Fig. 8) when 0.05 and $1 \mu\text{gC m}^{-3}$ were used for the a and b values, respectively, together with the rest of the parameters obtained from the PMF analysis (i.e., applying the parameters in the combination I in Table 3). Although these a and b values were used in the previous report and demonstrated reasonable agreement with the observations (i.e., ap-

plying the parameters in the combination III), the agreement was due to different f_{44} values and OM / OC ratios extracted from the PMF analysis (see the Sect. 3.4). To have reasonable agreement with the observations using the f_{44} and OM / OC extracted by the PMF analysis in Sect. 3.4, the use of 0.025 and $1 \mu\text{gC m}^{-3}$ for the a and b values (applying the parameters in the combination II) was found to give the best fitting to the observations.

As discussed previously, there was a strong relationship between the NO_x turn over and O_3 mixing ratio (Sect. 3.5.1). This relationship can be converted to the one between $t[\text{OH}]$ and O_3 mixing ratios (Fig. 9). An obtained linear relationship was $[\text{O}_3] = (3.48 \pm 0.06) \times 10^{-7} \times t[\text{OH}] + 30.7 \pm 0.3$. This provides the increasing rate of ozone $(3.48 \pm 0.06) \times 10^{-7} \times [\text{OH}] \text{ ppbv h}^{-1}$ and the background ozone mixing ratio of 30.7 ppbv in this region. If $[\text{OH}]$ of $5 \times 10^5 \text{ molecules cm}^{-3}$ (Takegawa et al., 2007; Irei et al., 2014) is given as the mean concentration of OH radical during the long-range transport in this region, the equation gives the average ozone production rate of $0.174 \text{ ppbv h}^{-1}$. A combination with measurements for OH radical concentration will secure a more accurate production rate of ozone in this region.

4 Summary

To improve our understanding of the ozone and SOA formation from the oxidation of atmospheric pollutants, we conducted field studies from December 2010 to May 2011 on Fukue Island, Nagasaki Prefecture, Japan. Wind-sector analysis of CO mixing ratios revealed that the ratio showed almost no wind-sector dependence, suggesting that the influence of emissions from residential areas near the measurement site was negligible. This fact in turn indicates that the influence of mid- and/or long-range transport of air pollutants to the site had a significant influence. Photochemical age, $t[\text{OH}]$, was estimated from $[\text{NO}_x]/[\text{NO}_y]$ and a NMHC concentration ratio, and the validity of the ratios was evaluated. The evaluation suggested that the hydrocarbon clock was significantly influenced by mixing with background air containing 0.16 ppbv of ethyne, a NMHC with a relatively long lifetime, resulting in significant bias in the estimation of $t[\text{OH}]$. In contrast, loss of NO_x due to reaction with O_3 at night was not influential to the NO_x/NO_y clock, which thus seemed to function appropriately, at least with respect to relative aging. The $t[\text{OH}]$ value obtained with the NO_x/NO_y clock was then compared with f_{44} obtained by AMS measurements, and f_{44} was observed to increase with increasing $t[\text{OH}]$, indicating the f_{44} can also be used as an oxidation indicator. This indicator likely works under the condition where two different types of organic aerosols, such as primary and secondary organic aerosols represented by hydrocarbon-like organic aerosols and low-volatile oxygenated organic aerosol, respectively, are mixed.

Using linear regression analysis, we estimated that the f_{44} increase rate for organic aerosols transported over the East China Sea averaged $(1.05 \pm 0.03) \times 10^{-9} \times [\text{OH}] \text{ h}^{-1}$. This rate was almost identical to the background-corrected rate of $1.3 \times 10^{-9} \times [\text{OH}] \text{ h}^{-1}$ observed during the New England Air Quality Study in the summer of 2002. The consistency may imply the production of similar SOA component(s), possibly humic-like substances. In addition, a clear proportional relationship was observed between O_3 and $t[\text{OH}]$. According to the linear regression analysis, the increase rate and background mixing ratio of O_3 in this region were found to be $(3.48 \pm 0.06) \times 10^{-7} \times [\text{OH}] \text{ ppbv h}^{-1}$ and 30.7 ppbv, respectively.

Data availability

Reference AMS mass spectra that were compared with our results were provided by I.M. Ulbrich, M. Lechner, and J.L. Jimenez, available at the following website: <http://cires.colorado.edu/jimenez-group/AMSsd/>

The Supplement related to this article is available online at doi:10.5194/acp-16-4555-2016-supplement.

Author contributions. Satoshi Irei contributed to the AMS, O_3 , and meteorological measurements and is the person in charge of the data analysis and writing the manuscript. Akinori Takami is the person in charge of the AMS, O_3 , and meteorological measurements. Yasuhiro Sadanaga is the person in charge of the NO_x and NO_y measurements. Seiichiro Yonemura is the person in charge of the CO measurements. Yoko Yokouchi is the person in charge of the NMHC measurements. Susumu Nozoe contributed to the NMHC measurements. Hiroshi Bandow contributed to the NO_x and NO_y measurements.

Acknowledgements. We acknowledge the NOAA Air Resources Laboratory (ARL) for the provision of the HYSPLIT transport and dispersion model and/or READY website (<http://www.ready.noaa.gov>). This project was financially supported by the Special Research Program from the National Institute for Environmental Studies, Japan (SR-95-2011). The project was partially supported by the International Research Hub Project for Climate Change and Coral Reef/Island Dynamics of University of the Ryukyus and the ESPEC Foundation for Global Environment Research and Technologies (Charitable Trust).

The article processing charges for this open-access publication were covered by the University of Bremen.

Edited by: C. von Savigny

References

- Allan, J. D., Delia, A. E., Coe, H., Bower, K. N., Alfarra, M. R., Jimenez, J. L., Middlebrook, A. M., Drewnick, F., Onasch, T. B., Canagaratna, M. R., Jayne, J. T., and Worsnop, D. R.: A generalized method for the extraction of chemically resolved mass spectra from Aerodyne aerosol mass spectrometer data, *J. Aerosol Sci.*, 35, 909–922, 2004.
- Brown, S. S., Ryerson, T. B., Wollny, A. G., Brock, C. A., Peltier, R., Sullivan, A. P., Weber, R. J., Dube, W. P., Trainer, M., Meagher, J. F., Fehsenfeld, F. C., and Ravishankara, A. R.: Variability in nocturnal nitrogen oxide processing and its role in regional air quality, *Science*, 311, 67–70, doi:10.1126/science.1120120, 2006.
- de Gouw, J. A., Middlebrook, A. M., Warneke, C., Goldan, P. D., Kuster, W. C., Roberts, J. M., Fehsenfeld, F. C., Worsnop, D. R., Canagaratna, M. R., Pszenny, A. A. P., Keene, W. C., Marchewka, M., Bertman, S. B., and Bates, T. S.: Budget of organic carbon in a polluted atmosphere: Results from the New England Air Quality Study in 2002, *J. Geophys. Res.-Atmos.*, 110, D16305, doi:10.1029/2004JD005623, 2005.
- Draxler, R. R. and Rolph, G. D.: HYSPLIT (Hybrid Single-Particle Lagrangian Integrated Trajectory) Model Access via NOAA ARL READY. NOAA Air Resources Laboratory, College Park, MD, available at: <http://www.arl.noaa.gov/HYSPLIT.php>, 2013.
- Ebben, C. J., Strick, B. F., Upshur, M. A., Chase, H. M., Achtyl, J. L., Thomson, R. J., and Geiger, F. M.: Towards the identification of molecular constituents associated with the surfaces of isoprene-derived secondary organic aerosol (SOA) particles, *Atmos. Chem. Phys.*, 14, 2303–2314, doi:10.5194/acp-14-2303-2014, 2014.
- Finlayson-Pitts, B. J. and Pitts Jr. J. N.: Chemistry of the upper and lower atmosphere, Academic Press, San Diego, California, USA, 2000.
- Grosjean, D. and Seinfeld, J. H.: Parameterization of the formation potential of secondary organic aerosols, *Atmos. Environ.*, 23, 1733–1747, 1989.
- Irei, S., Huang, L., Collin, F., Zhang, W., Hastie, D., and Rudolph, J.: Flow reactor studies of the stable carbon isotope composition of secondary particulate organic matter generated by OH-radical induced reaction of toluene, *Atmos. Environ.*, 40, 5858–5867, 2006.
- Irei, S., Rudolph, J., Huang, L., Auld, J., and Hastie, D.: Stable carbon isotope ratio of secondary particulate organic matter formed by photooxidation of toluene in indoor smog chamber, *Atmos. Environ.*, 45, 856–862, 2011.
- Irei, S., Takami, A., Hayashi, M., Sadanaga, Y., Hara, K., Kaneyasu, N., Sato, K., Arakaki, T., Hatakeyama, S., Bandow, H., Hikida, T., and Shimono, A.: Transboundary secondary organic aerosol in western Japan indicated by the $\delta^{13}\text{C}$ of water-soluble organic carbon and the m/z 44 signal in organic aerosol mass spectra, *Environ. Sci. Technol.*, 48, 6273–6281, 2014.
- Irei, S., Takami, A., Sadanaga, Y., Miyoshi, T., Arakaki, T., Sato, K., Kaneyasu, N., Bandow, H., and Hatakeyama, S.: Transboundary secondary organic aerosol in western Japan: An observed limitation of the f_{44} oxidation indicator, *Atmos. Environ.*, 120, 71–75, 2015.
- Jayne, J. T., Leard, D. C., Zhang, X., Davidovits, P., Smith, K. A., Kolb, C. E., and Worsnop, D. R.: Development of an aerosol mass spectrometer for size and composition analysis of submicron particles, *Aerosol Sci. Technol.*, 33, 49–70, 2000.
- Jimenez, J. L., Canagaratna, M. R., Donahue, N. M., Prevot, A. S. H., Zhang, Q., Kroll, J. H., DeCarlo, P. F., Allan, J. D., Coe, H., Ng, N. L., Aiken, A. C., Docherty, K. D., Ulbrich, I. M., Grieshop, A. P., Robinson, A. L., Duplissy, J., Smith, J. D., Wilson, K. R., Lanz, V. A., Hueglin, C., Sun, Y. L., Laaksonen, A., Raatikainen, T., Rautiainen, J., Vaattovaara, P., Ehn, M., Kulmala, M., Tomlinson, J. M., Collins, D. R., Cubison, M. J., Dunlea, E. J., Huffman, J. A., Onasch, T. B., Alfarra, M. R., Williams, P. I., Bower, K., Kondo, Y., Schneider, J., Drewnick, F., Borrmann, S., Weimer, S., Demerjian, K., Salcedo, D., Cottrell, L., Griffin, R., Takami, A., Miyoshi, T., Hatakeyama, S., Shimono, A., Sun, J. Y., Zhang, Y. M., Dzepina, K., Kimmel, J. R., Sueper, D., Jayne, J. T., Herndon, S. C., Trimborn, A. M., Williams, L. R., Wood, E. C., Kolb, C. E., Baltensperger, U., and Worsnop, D. R.: Evolution of organic aerosols in the atmosphere, *Science*, 326, 1525–1529, 2009.
- Kanaya, Y., Tanimoto, H., Yokouchi, Y., Taketani, F., Komazaki, Y., Irie, H., Takashima, H., Pan, X., Nozoe, S., and Inomata, S.: Diagnosis of photochemical ozone production rates and limiting factors in continental outflow air masses reaching Fukue Island, Japan: Ozone-control implications, *Aerosol Air Qual. Res.*, 16, 430–441, 2016.
- Kato, S., Kajii, Y., Itokazu, R., Hirokawa, J., Koda, S., and Kinjo, Y.: Transport of atmospheric carbon monoxide, ozone, and hydrocarbons from Chinese coast to Okinawa Island in the western Pacific during winter, *Atmos. Environ.*, 38, 2975–2981, 2004.
- Kim, C.-H., Park, S.-Y., Kim, Y.-J., Chang, L.-S., Song, S.-K., Moon, Y.-S., and Song, C.-K.: A numerical study on indicators of long-range transport potential for anthropogenic particulate matters over northeast Asia, *Atmos. Environ.*, 58, 35–44, 2012.
- Kleinman, L. I., Daum, P. H., Lee, Y.-N., Senum, G. I., Springston, S. R., Wang, J., Berkowitz, C., Hubbe, J., Zaveri, R. A., Brechtel, F. J., Jayne, J., Onasch, T. B., and Worsnop, D.: Aircraft observations of aerosol composition and ageing in New England and Mid-Atlantic States during the summer 2002 New England Air Quality Study field campaign, *J. Geophys. Res.-Atmos.*, 112, D09310, doi:10.1029/2006JD007786, 2007.
- Kurokawa, J., Ohara, T., Morikawa, T., Hanayama, S., Janssens-Maenhout, G., Fukui, T., Kawashima, K., and Akimoto, H.: Emissions of air pollutants and greenhouse gases over Asian regions during 2000–2008: Regional Emission inventory in ASia (REAS) version 2, *Atmos. Chem. Phys.*, 13, 11019–11058, doi:10.5194/acp-13-11019-2013, 2013.
- Liggio, J., Li, S.-M., Vlasenko, A., Sjostedt, S., Chang, R., Shantz, N., Abbatt, J., Slowik, J. G., Bottenheim, J. W., Brickell, P. C., Strond, C., and Leaitch, R. W.: Primary and secondary organic aerosols in urban air masses intercepted at a rural site, *J. Geophys. Res.-Atmos.*, 115, D21305, doi:10.1029/2010JD014426, 2010.
- McKeen, S. A. and Liu, S. C.: Hydrocarbon ratios and photochemical history of air masses, *Geophys. Res. Lett.*, 20, 2363–2366, 1993.
- Ng, N. L., Canagaratna, M. R., Zhang, Q., Jimenez, J. L., Tian, J., Ulbrich, I. M., Kroll, J. H., Docherty, K. S., Chhabra, P. S., Bahreini, R., Murphy, S. M., Seinfeld, J. H., Hildebrandt, L., Donahue, N. M., DeCarlo, P. F., Lanz, V. A., Prévôt, A. S. H., Dinar, E., Rudich, Y., and Worsnop, D. R.: Organic aerosol

- components observed in Northern Hemispheric datasets from Aerosol Mass Spectrometry, *Atmos. Chem. Phys.*, 10, 4625–4641, doi:10.5194/acp-10-4625-2010, 2010.
- Olszyna, K. J., Bailey, E. M., Simonaitis, R., and Meagher, J. F.: O_3 and NO_y relationships at a rural site, *J. Geophys. Res.-Atmos.*, 99, 14557–14563, 1994.
- Pandey Deolal, S., Brunner, D., Steinbacher, M., Weers, U., and Staehelin, J.: Long-term in situ measurements of NO_x and NO_y at Jungfraujoch 1998–2009: time series analysis and evaluation, *Atmos. Chem. Phys.*, 12, 2551–2566, doi:10.5194/acp-12-2551-2012, 2012.
- Parrish, D. D., Hahn, C. J., Williams, E. J., Norton, R. B., and Fehsenfeld, F. C.: Indications of photochemical histories of Pacific air masses from measurements of atmospheric trace species at Point Arena, California, *J. Geophys. Res.-Atmos.*, 97, 15883–15901, 1992.
- Parrish, D. D., Trainer, M., Hereid, D., Williams, E. J., Olszyna, K. J., Harley, R. A., Meagher, J. F., and Fehsenfeld, F. C.: Decadal change in carbon monoxide to nitrogen oxide ratio in U.S. vehicular emissions, *J. Geophys. Res.-Atmos.*, 107, 4140, doi:10.1029/2001JD000720, 2002.
- Pochanart, P., Akimoto, H., Kinjo, Y., and Tanimoto, H.: Surface ozone at four remote island sites and the preliminary assessment of the exceedances of its critical level in Japan, *Atmos. Environ.*, 36, 4235–4250, 2002.
- Roberts, J. M., Fehsenfeld, F. C., Liu, S. C., Bollinger, M. J., Hahn, C., Albritton, D. L., and Sievers, R. E.: Measurements of aromatic hydrocarbon ratios and NO_x concentrations in the rural troposphere: Observations of air mass photochemical aging and NO_x removal, *Atmos. Environ.*, 18, 2414–2432, 1984.
- Roussel, P. B., Lin, X., Camacho, F., Laszlo, S., Taylor, R., Melo, O., Shepson, P. B., Hastie, D., and Melo, O. T.: Observations of ozone and precursor levels at two sites around Toronto, Ontario, during SONTOS 92, *Atmos. Environ.*, 30, 2145–2155, 1996.
- Rudolph, J. and Johnen, F. J.: Measurements of light atmospheric hydrocarbons over the Atlantic in regions of low biological activity, *J. Geophys. Res.-Atmos.*, 95, 20583–20591, 1990.
- Sadanaga, Y., Fukumori, Y., Kobashi, T., Nagata, M., Takenaka, N., and Bandow, H.: Development of a selective light-emitting diode photolytic NO_2 converter for continuously measuring NO_2 in the atmosphere, *Anal. Chem.*, 82, 9234–9239, 2010.
- Seinfeld, J. H. and Pandis, S. N.: *Atmospheric Chemistry and Physics*, A Wiley Interscience Publication, New York, USA, 1997.
- Suthawaree, J., Kato, S., Takami, A., Kadena, H., Toguchi, M., Yogi, K., Hatakeyama, S., and Kajii, Y.: Observation of ozone and carbon monoxide at Cape Hedo, Japan: Seasonal variation and influence of long-range transport, *Atmos. Environ.*, 42, 2971–2981, 2008.
- Takami, A., Miyoshi, T., Shimono, A., and Hatakeyama, S.: Chemical composition of fine aerosol measured by AMS at Fukue Island, Japan during APEX period, *Atmos. Environ.*, 39, 4913–4924, 2005.
- Takami, A., Miyoshi, T., Shimono, A., Kaneyasu, N., Kato, S., Kajii, Y., and Hatakeyama, S.: Transport of anthropogenic aerosols from Asia and subsequent chemical transformation, *J. Geophys. Res.-Atmos.*, 112, D22S31, doi:10.1029/2006JD008120, 2007.
- Takegawa, N., Kondo, Y., Koike, M., Chen, G., Machida, T., Watai, T., Blake, D. R., Streets, D. G., Woo, J.-H., Carmichael, G. R., Kita, K., Miyazaki, Y., Shirai, T., Liley, J. B., and Ogawa, T.: Removal of NO_x and NO_y in Asian outflow plumes: Aircraft measurements over the western Pacific in January 2002, *J. Geophys. Res.-Atmos.*, 109, D23S04, doi:10.1029/2004JD004866, 2004.
- Takegawa, N., Miyakawa, T., Kondo, Y., Blake, D. R., Kanaya, Y., Koike, M., Fukuda, M., Komazaki, Y., Miyazaki, Y., Shimono, A., and Takeuchi, T.: Evolution of submicron organic aerosol in polluted air exported from Tokyo, *Geophys. Res. Lett.*, 33, D11206, doi:10.1029/2006GL025815, 2006.
- Tagiguchi, Y., Takami, A., Sadanaga, Y., Lun, X., Shimizu, A., Matsui, I., Sugimoto, N., Wang, W., Bandow, H., and Hatakeyama, S.: Transport and transformation of total reactive nitrogen over the East China Sea, *J. Geophys. Res.-Atmos.*, 113, D10306, doi:10.1029/2007JD009462, 2008.
- Tang, J. H., Chan, L. Y., Chang, C. C., Liu, S., and Li, Y. S.: Characteristics and sources of non-methane hydrocarbons in background atmospheres of eastern, southwestern, and southern China, *J. Geophys. Res.-Atmos.*, 114, D03304, doi:10.1029/2008JD010333, 2009.
- Tanimoto, H., Sawa, Y., Yonemura, S., Yumimoto, K., Matsueda, H., Uno, I., Hayasaka, T., Mukai, H., Tohjima, Y., Tsuboi, K., and Zhang, L.: Diagnosing recent CO emissions and ozone evolution in East Asia using coordinated surface observations, adjoint inverse modeling, and MOPITT satellite data, *Atmos. Chem. Phys.*, 8, 3867–3880, doi:10.5194/acp-8-3867-2008, 2008.
- Ulbrich, I. M., Canagaratna, M. R., Zhang, Q., Worsnop, D. R., and Jimenez, J. L.: Interpretation of organic components from Positive Matrix Factorization of aerosol mass spectrometric data, *Atmos. Chem. Phys.*, 9, 2891–2918, doi:10.5194/acp-9-2891-2009, 2009.
- Ulbrich, I. M., Lechner, M., and Jimenez, J. L.: AMS Spectral Database, available at: <http://cires.colorado.edu/jimenez-group/AMSsd/>, last access: October 2015.
- Yokouchi, Y.: Development of real-time monitoring system for non-methane hydrocarbons in the atmosphere, Final Report for Environmental Technology Development Fund, Ministry of the Environment, 2008 (in Japanese).
- Yokouchi, Y., Takami, A., and Ohara, T.: Observational and modeling study of the high-ozone episode in northern Kyusyu focused on the impact of ozone precursors, Report of Special Research from the National Institute for Environmental Studies, Japan, 2011 (in Japanese).
- Yuba, A., Sadanaga, Y., Takami, A., Hatakeyama, S., Takenaka, N., and Bandow, H.: Measurement system for particulate nitrate based on the scrubber difference $NO-O_3$ chemiluminescence method in remote areas, *Anal. Chem.*, 82, 8916–8921, 2010.
- Wang, M., Shao, M., Chen, W., Lu, S., Liu, Y., Yuan, B., Zhang, Q., Zhang, Q., Chang, C.-C., Wang, B., Zeng, L., Hu, M., Yang, Y., and Li, Y.: Trends of non-methane hydrocarbons (NMHC) emissions in Beijing during 2002–2013, *Atmos. Chem. Phys.*, 15, 1489–1502, doi:10.5194/acp-15-1489-2015, 2015.
- Zhang, Q., Worsnop, D. R., Canagaratna, M. R., and Jimenez, J. L.: Hydrocarbon-like and oxygenated organic aerosols in Pittsburgh: insights into sources and processes of organic aerosols, *Atmos. Chem. Phys.*, 5, 3289–3311, doi:10.5194/acp-5-3289-2005, 2005.